Applied Energy 280 (2020) 115952

Contents lists available at ScienceDirect

Applied Energy

journal homepage: www.elsevier.com/locate/apenergy

Hull geometry optimisation of wave energy converters: On the choice of the optimisation algorithm and the geometry definition

Anna Garcia-Teruel [a,*], Bryony DuPont [b], David I.M. Forehand [a]

[a] Institute for Energy Systems, School of Engineering, The University of Edinburgh, Edinburgh, EH9 3BF, United Kingdom
[b] School of Mechanical, Industrial, and Manufacturing Engineering, Oregon State University, Corvallis, OR, 97331, USA

ARTICLE INFO

Keywords:
Wave Energy Converter
Optimisation algorithms
Hull
Geometry
Design

ABSTRACT

It is key in the development of wave energy systems to aim at designing economically competitive solutions that enable maximal annual energy production. Previous studies identify the Wave Energy Converter (WEC) structure, i.e. the hull, to have one of the largest cost reduction potentials. Due to this potential, geometry optimisation of WECs has been previously considered, however, most of these studies have been limited by the simplicity of the employed geometrical shapes and the lack of accurate cost models. It is, therefore, important to include an adaptable geometry definition capable of generating diverse WEC shapes, and to account for other factors that can have an effect on costs. These considerations result in a more challenging optimisation problem, and a more complex objective function. The goal of this study is to address the challenge of finding a suitable and efficient optimisation method for WEC geometry design. In this paper, different geometry definitions, such as using simple shapes or B-spline surfaces, and different meta-heuristic optimisation algorithms, such as genetic algorithms or particle swarm optimisation are applied to this problem to find the most suitable choices. Results show an improvement in final objective function values of up to 224% when using an adaptable geometry definition and up to 11% when employing the most suitable optimisation algorithm compared to previous results. In conclusion, the choice of the different elements of the optimisation formulation have a large impact on the quality of the optimisation results and should be based on preliminary studies as presented here.

1. Introduction

High energy potential is found in ocean waves. For this reason, many different types of Wave Energy Converters (WECs) have been developed, with the goal of designing devices with reduced costs and increased annual energy production. Design optimisation offers the opportunity to explore more of the design space while avoiding expensive build and test iterations and it has been used to improve energy efficiency of a range of commercially developed systems. It has been applied, for example, to improve efficiency of buildings [1], hybrid solar-wind generation plants [2], also in combination with storage technologies [3], or Combined Cooling, Heating and Power (CCHP) systems [4]. This type of design optimisation is particularly relevant for emerging technologies such as wave energy converters, where improved early stage designs have a great impact on technology advancement towards commercialisation.

From previous studies, it is known that one of the largest cost reduction potentials is associated with the Wave Energy Converter (WEC) structure, i.e. the hull [5,6]. Apart from the high capital expenditure associated with the device hull, the geometry of the hull is crucial for the device hydrodynamics, and thus for the annual energy production. The cost reduction potential and key hydrodynamic characteristics associated to the device hull have resulted in a number of device hull geometry optimisation studies, which not only aim at maximising performance, but also minimising costs. A point absorber based on simple hull shapes using cylindrical geometries was studied by Gilloteaux et al. in [7] to understand the effect of different control strategies on optimal device size. Kurniawan et al. optimised dumbbell-like shapes in [8] considering their total surface area as a proxy for costs. In [9] using a similar methodology, they optimised an oscillating wave surge device, where the position of the axis of rotation was also considered as an optimisation variable. Costello et al. [10] optimised a barge-shaped device using a detailed cost model versus a maximising energy absorption only approach. Other types of devices such as two-body point absorbers were optimised in a multi-objective optimisation set-up by Blanco et al. in [11]. Oscillating Water Columns (OWC) have also been extensively studied by Weber et al. for example, in [12]. Power Take-Off (PTO) systems and the applied control strategies are

* Corresponding author.
E-mail address: a.garcia-teruel@ed.ac.uk (A. Garcia-Teruel).

https://doi.org/10.1016/j.apenergy.2020.115952
Received 27 May 2020; Received in revised form 18 September 2020; Accepted 26 September 2020
Available online 28 October 2020

Nomenclature

b	Half beam (m)
d	Draft (m)
f	Objective function (NA)
g	Gravitational acceleration (m/s^2)
C_a	Added damping (kg/s, (kg m)/s, or (kg m^2)/s)
H_{m0}	Significant wave height (m)
M_a	Added mass (kg, kg m, or kg m^2)
MaxGen	Maximum number of iterations defined for an optimisation (NA)
N_{Elite}	Number of elite individuals used for reinsertion in genetic algorithm (NA)
N_{Ind}	Number of individuals in genetic algorithm (NA)
N_{Pair}	Number of pairings in genetic algorithm (NA)
$N_{Parents}$	Number of parents in genetic algorithm (NA)
$\bar{P}$	Mean annual power (W)
P_{pm}	Power per metre crest length (W/m)
r	Radius (m)
S	Submerged surface area (m^2)
T_e	Energy period (s)
V	Submerged volume (m^3)
v_n	Vertex (NA)
w	Half width (m)
$\mathbf{Z}$	Device's intrinsic impedance matrix (kg/s, (kg m)/s, and (kg m^2)/s)
$\mathbf{Z}_c$	Control impedance matrix (kg/s, (kg m)/s, and (kg m^2)/s)
$\mathbf{x}$	Vector of decision variables (NA)
λ	Wavelength (m)
φ	Acceleration constants in particle swarm optimisation algorithm (NA)
ω_e	Energy frequency of the sea state (rad/s)
ξ	Device oscillation (m)
AES	Average number of Evaluations to a Solution (NA)
CW	Capture Width (m)
CWR	Capture Width Ratio (%)
DoF	Degree of Freedom (NA)
GA	Genetic Algorithm (NA)
MBF	Mean Best Fitness (NA)
PSO	Particle Swarm Optimisation (NA)
PTO	Power Take-Off (NA)
SR	Success Rate (NA)
WEC	Wave Energy Converter (NA)

also known to have a large impact on system dynamics and the potential for cost reduction [5]. These systems have been extensively studied and optimised, and some studies exist which simultaneously optimise geometry and PTO-parameters, such as the one previously mentioned by Gilloteaux et al. [7]. Due to their potential impact on system dynamics and structural loads mooring lines have also been optimised, for example, in [13].

All of the above studies used geometry definitions based on simple shapes such as cylinders, barges or ellipsoids. An approach capable of generating very diverse shapes was developed by McCabe et al. using a more complex geometry definition based on B-spline surfaces. An initial method applied to a surging and pitching device was presented in [14]. The method was further developed and applied to a surging only device in [15], where geometries were optimised using a single-objective genetic algorithm. Shapes were optimised to maximise mean annual absorbed power, and mean annual absorbed power in combination with the submerged volume. Complex shapes with high curvatures and thin cross-sections resulted from optimisations using submerged volume in the objective function, which might not be cost-effective to manufacture.

Results from previous studies are limited by the choice of geometry definition and valid only for specific conditions. That is, resulting shapes might just be optimal for very specific sea conditions, within previously selected base shapes (e.g. cylinders), and for specific modes for power extraction; and they may not be cost-effective to manufacture. It is, therefore, important to be able to generate a diverse range of improved WEC designs while considering costs, in order to explore more of the design space and identify promising solutions. Having a more flexible and comprehensive optimisation set-up, however, makes the optimisation problem more challenging, since the number of optimisation variables and constraints is increased, and the objective function can become more complex and time consuming to calculate. Ensuring convergence to a near globally optimal shape, and achieving this within an acceptable timescale, is not trivial and requires a thorough exploration of the optimisation algorithm.

There is a clear need for the development of a flexible and comprehensive method for hull geometry optimisation, due to the relevance of design optimisation tools at early design stages, the high cost associated with the structure and the lack of a general methodology and best practices for WEC geometry optimisation. As previously identified by Weber et al. in [16], this is key for the advancement of wave energy technologies. Such a method for hull geometry optimisation represents a fundamental design aid for technology developers, but it can also serve funding bodies to assess different technologies, since it will build on a methodology for design comparison.

The present paper addresses this gap by finding a suitable and efficient optimisation method for WEC geometry optimisation. With this purpose, the geometry definition and the choice of the optimisation algorithm are studied. Different geometry definitions are compared: a hemisphere, a vertical cylinder, a barge and bi-cubic B-spline surfaces. In addition, different objective functions are considered based on the mean annual power $\bar{P}$, the submerged volume V, and the submerged surface area S ($\bar{P}$, $\frac{\bar{P}}{V^{\frac{1}{3}}}$, $\frac{\bar{P}}{V^{\frac{2}{3}}}$, $\frac{\bar{P}}{V}$, $\frac{\bar{P}}{S}$, and $\frac{\bar{P}}{S^{\frac{1}{2}}}$), for a device oscillating in surge only, and in surge, heave and pitch. To find the most suitable optimisation algorithm for each case, a range of meta-heuristic algorithms are applied to this problem, including different single-objective Particle Swarm Optimisation (PSO) and Genetic Algorithm (GA) implementations.

First, the general formulation of the optimisation problem is introduced in Section 2.1 and some background is provided in Section 2.2 by introducing the method developed by McCabe in [14,15] capable of generating very diverse shapes, and which serves as a starting point for this study. The required assumptions and the verification of the re-implemented method are briefly discussed in Sections 2.3 and 2.4, respectively. The extensions that were used to increase its robustness are presented in Section 2.5. The enhanced method introduced here is used as a baseline to analyse two main elements of the optimisation process: the optimisation algorithms and the geometry definition. The approach and studied cases employed to investigate the most suitable optimisation algorithm and geometry definition for wave energy converter geometry optimisation are introduced in Section 3. The obtained results are then discussed in Section 4, where first the most suitable algorithm for each of the studied cases is identified, and then these are applied to optimisation approaches using different geometry definitions. The main conclusions drawn from this study are presented in Section 5.

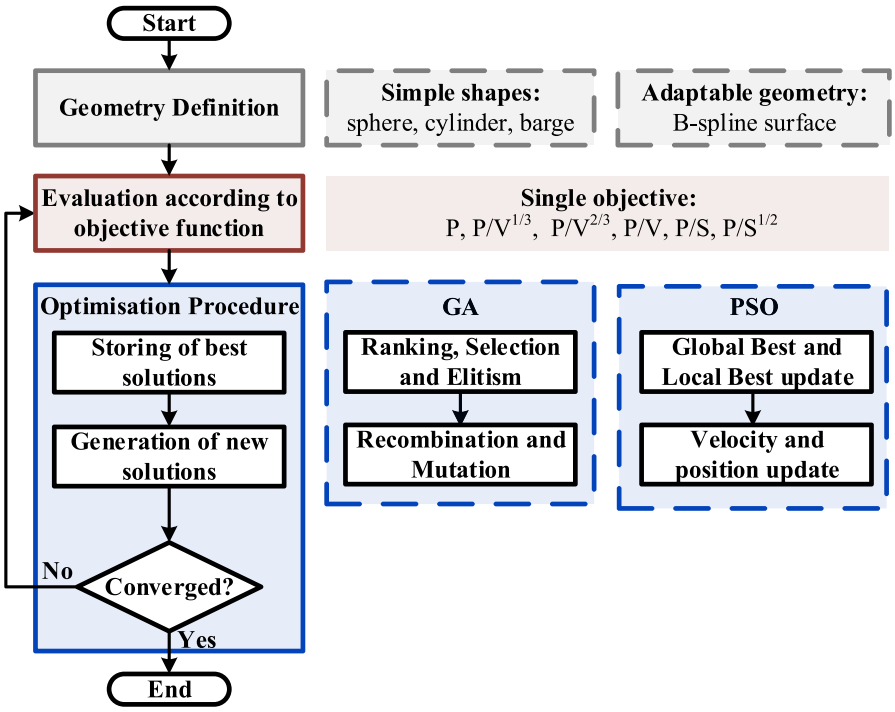

Fig. 1. Flow chart of the optimisation procedure, showing an overview of the studied elements. Both simple shapes and adaptable geometry definitions, as well as, Genetic Algorithms (GA) and Particle Swarm Optimisation (PSO) algorithms are investigated in this study [17].

2. Methodology

In this section, the basic formulation of the optimisation problem is introduced. To be able to study the suitability of geometry definition and optimisation algorithms for wave energy converter geometry optimisation, a baseline method was used. Its implementation is discussed in this section. The method was re-implemented based on two publications [14,15]. Further considerations, not mentioned in those two publications, were found necessary for the correct functioning of the optimisation. Additionally, the original implementation was applied to a surging only device, whereas the implementation used here applies to devices oscillating in any degree of freedom or combination of degrees of freedom. Although this is not the focus of this paper, the main characteristics of this re-implemented method and an overview of the additionally required considerations are introduced in the following for context and to facilitate reproducibility.

2.1. Optimisation problem

A single objective optimisation problem is defined as a problem in which the optimal values for a number of decision variables x_i are searched so that an objective function $f(\mathbf{x})$ is minimised or maximised. The search space Ω, i.e. the full range of possible decision variable values, is constrained through bounds and non-linear constraints defining restrictions between certain variable combinations. The solution space Δ i.e. the space of feasible solutions for the studied objective function, can be constrained by various equality g_j and inequality h_k constraints. This is represented mathematically below in the standard form [18].

$$\begin{aligned} &\min f(\mathbf{x}) \\ &\text{objective function:} && f(\mathbf{x}), \quad \text{for} \quad f \in \Delta \\ &\text{decision variable:} && \mathbf{x} = \{x_1, \ldots, x_m\} \in \Omega \\ &\text{equality constraint:} && g_j(x) = 0 \quad \text{for} \quad j = 1, \ldots, n \\ &\text{inequality constraint:} && h_k(x) \leq 0 \quad \text{for} \quad k = 1, \ldots, o \end{aligned} \tag{1}$$

A WEC geometry optimisation process is characterised by the way the geometry is defined (including the decision variables), the objective function(s) used to evaluate the generated geometries, and the optimisation algorithms applied to select geometries and generate improved ones. An overview of the geometry optimisation process is given in Fig. 1. Each of the main steps represented in this figure are introduced in the subsequent sections.

The focus of this paper is to study the suitability of different geometry definitions and optimisation algorithms. The studied areas are marked in Fig. 1 with dashed lines. The considered geometry definitions comprise a hemisphere, a vertical cylinder, a barge and bi-cubic B-spline surfaces. GA and PSO algorithms are applied to the single-objective optimisation problem.

2.2. Re-implemented method

The method introduced by McCabe in [15] is used as a reference, due to the ability of this method to generate very diverse shapes free of designer bias.

Geometry definition

The WEC hull geometry is defined based on a polyhedron with an x–z-symmetry plane. As shown in Fig. 2, the corner points are used as vertices, between which further control points are defined through interpolation. The surface is then approximated by bicubic B-spline surfaces. Some of the vertices' coordinates are fixed, since the vertices lie on the free surface or on the symmetry plane, but the rest (22 in total) can be changed randomly within defined ranges. Note that spherical coordinates (r_n, θ_n, ϕ_n) are used for each vertex V_n.

Geometry evaluation according to the objective function

In McCabe's original implementation [15] shapes were optimised to maximise $\bar{P}$, $\bar{P}/V$ and $\bar{P}/\sqrt[3]{V}$. All objective functions, hence, include the mean annual power $\bar{P}$, produced by the wave energy converter. The power calculation procedure, as well as the scatter diagram for the considered location can be found in [15]. The hydrodynamic model and the transfer of the method in [15] to a multiple modes-of-motion oscillating WEC is presented in [19]. An overview is provided here for completeness. The hydrodynamic model is based on the assumptions

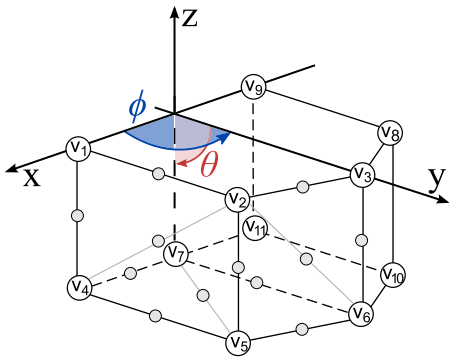

Fig. 2. Geometry definition based on a polyhedron with numbered vertices V_n and vertex coordinates (r_n, θ_n, ϕ_n). Additionally, some example representations of interpolated points are shown in grey [17], adapted from Figure 1 in [15].

that ocean waves can be described using potential flow theory (i.e. irrotational flow, and inviscid and incompressible fluid), wave heights are small relative to the wave length, and body oscillations are also small. This means that linear wave theory can be applied, and the system oscillations can be described as the superposition of multiple harmonic oscillations. Furthermore, the system is assumed to have reached steady-state oscillatory motion. Based on these assumptions the system can be described in the frequency domain.

The mean annual power is calculated for a particular site and WEC geometry. The wave energy resource is represented with irregular uni-directional waves in a fully developed sea using a Bretschneider spectrum [20]. The algorithm is implemented in Matlab and uses WAMIT – a frequency-domain programme based on a Boundary Element Method (BEM) – to calculate the hydrodynamic characteristics for each shape based on the frequencies selected to represent the spectrum. A frequency range from 0.02 to 3 rad/s is considered. The yearly average power is obtained with the sea states occurrence matrix. The volume for each geometry can be obtained from WAMIT.

For power absorption, a semi-optimal linear control is used, that brings the device's natural frequency to match the energy frequency of the sea state $\omega_e = \frac{2\pi}{T_e}$ calculated as in [21]. The corresponding control force is composed of constant inertia, damping and stiffness terms, which are defined according to [22] so that the control impedance matrix $\mathbf{Z}_c$ equals the complex conjugate of the device's intrinsic impedance $\mathbf{Z}^*$ at the energy period, where $*$ denotes complex conjugate. The application of this control strategy results in an equation of motion which is independent of the hull's inertia and hydrostatic stiffness.

Despite using a frequency-domain hydrodynamic model, the time series of the device oscillation and of the instantaneous power are calculated to be able to apply stroke and PTO rating constraints. The instantaneous power absorbed by the PTO is set to zero if the device oscillation is outside of the predefined stroke limits, and is set to the maximum power limit given by the PTO rating, if this rating is exceeded. This analysis is performed for N time steps with $\Delta t = 0.2$ s and $t_N \approx \frac{2\pi}{\Delta\omega}$. This results in a non-repeating time series.

The geometry is considered to be an infeasible solution, if the final annual power production is negative or if it exceeds the maximum capture width $C_{W,MAX}$ of an axisymmetric body for the available power per metre crest length. $C_{W,MAX}$ can be calculated for different combinations of modes of motion according to [22]. For the surge; and surge, heave and pitch cases studied, $C_{W,MAX}$ equals λ/π and $3\lambda/\pi$, respectively. λ here represents the wavelength calculated from the energy period for each sea state. Although the bodies considered in the present implementation are not axisymmetric, this upper bound also serves the present case by ensuring that the calculated average power per sea state does not surpass the theoretical limit of average power available in the sea.

Parameter constraints

Parameter constraints common to all optimisation problems are summarised here. PTO stroke constraints $\xi_{MIN}(i)$ and $\xi_{MAX}(i)$ are applied on each degree-of-freedom. In addition, a PTO rating $P_{PTO,MAX}$ is enforced. The device's submerged volume V is constrained to avoid the optimisation to converge into very large or very small shapes. The mean power production is restricted by the capture width $C_{W,MAX}$ of an axisymmetric body depending on the modes of motion and the power per metre crest length P_{pm} available in the considered sea state. These constraints are listed below and, when applicable, they were mentioned at the corresponding stage of the geometry evaluation.

$$\begin{aligned}
\xi_{MAX}(i) &= 5\text{ m}; 10\text{ m} \quad | i = 1,2,3\\
\xi_{MAX}(i) &= \pi/4 \quad | i = 4,5,6\\
\xi_{MIN}(i) &= -\xi_{MAX}(n) \quad | i = 1,2,3,4,5,6\\
P_{PTO,MAX} &= 2.5\text{ MW}; 5\text{ MW}\\
250\text{ m}^3 &\le V \le 4000\text{ m}^3\\
0\text{ MW} &\le \bar{\mathbf{P}} \le C_{W,MAX}\cdot P_{pm}
\end{aligned}$$

From the results in [15] it can be observed that differences in $\xi_{MAX}(i)$ and $P_{PTO,MAX}$ result in larger or lower mean annual power production values, but do not have a significant effect on the resulting shapes. For this reason, if not otherwise specified, $\xi_{MAX}(i) = 5$ m $| i = 1,2,3$ and $P_{PTO,MAX} = 2.5$ MW were used for the optimisation runs performed within this study.

Optimisation procedure

In the previously mentioned studies, both meta-heuristic optimisation methods such as genetic algorithms [8,9,14,15,23], and evolutionary algorithms [11] have been used. Additionally, exact methods based on direct search approaches, such as the simplex algorithm [7] or the simple pattern search [10] have been applied. Gomes et al. [24] apply both exact and meta-heuristic methods to the geometry optimisation problem. For problems with a reduced number of optimisation variables, as was the case in [7] and [24], exact methods might be able to provide optimal solutions with less computational effort. However, as the geometry definition and the objective function become more complex, meta-heuristic methods have a high potential to perform better, as they have proven to be more suitable for finding good enough solutions for complex problems within an acceptable time scale [25]. That is, in cases where the objective function has multiple maxima and minima, meta-heuristic algorithms have proven to perform a more effective search of the solution space and to be more likely to find global optima when compared for instance to gradient-based methods. Through their strategic stochastic approach, meta-heuristic algorithms are less dependent on previously analysed solutions. Additionally, in cases where the objective function is not differentiable, for example, due to discontinuities caused by the applied constraints, gradient methods cannot be employed. It was also discussed in [26], that meta-heuristic methods are particularly suitable for this application when compared to gradient-based methods, due to spurious oscillations found in the objective function, as a result of the numerical approximations employed in the hydrodynamic model.

In the original implementation, genetic algorithms are used which are based on evolution theory featuring the survival of the fittest individuals within a population. The initial population – composed of a defined number of individuals (N_{Ind}) – is a set of WEC shapes, in this case, represented by random combinations of the optimisation variables described earlier. The geometries are assessed based on the objective function and are assigned a fitness value according to Baker's linear ranking algorithm [27]. A number of individuals in each generation are selected through Stochastic Universal Sampling to pair by Intermediate Recombination [28] ($N_{Parents}$), which create a defined number of new individuals – depending on the number of pairings per individual ($N_{Pairings}$) – that will carry forward their genetic information. Some

characteristics of these new individuals are mutated using the Breeder Genetic Algorithm Mutation [28] with a mutation rate of three over the number of variables (N_{vars}) to ensure that further characteristics that might improve the individual's fitness and that were not present in the first generation can be evaluated. Mutation helps to search more of the solution space and avoids convergence on a particular local optimum. To keep all characteristics of the best performing individuals in the following generations, a number of the fittest individuals of the assessed generation (N_{Elite}) are reinserted in the following one — this is known as Elite Reinsertion. To keep the population size constant throughout all generations only $N_{Ind} - N_{Elite}$ children are selected for reinsertion. The new generation is then again assessed based on the objective function. In the original implementation this process was iterated 50 times in four separate optimisation runs, and the 22 best individuals of the four runs were then used in a further optimisation run with 50 more generations. This involves 5010 function evaluations.

2.3. Implementation details and assumptions

The higher-order method in WAMIT was employed, which uses B-splines instead of piecewise-constant values across discretisation areas to represent the velocity potential on surfaces in a continuous manner. To achieve this, the characteristics of the employed B-splines need to be defined. Splines of order $k = 4$ are used, and the orders of Gauss quadrature used for the inner and outer integrations are defined based on this as k and $k+1$, respectively, as described in the manual [29]. The number of subdivisions defined in WAMIT is equivalent to the number of knot spans in a B-spline. See [30] for the used B-spline definition in WAMIT, which is based on [31].

In [15], McCabe mentions the use of the iterative solver in WAMIT. However, when using the higher-order method, the WAMIT manual [29] does not recommend the use of the iterative solver, due to a decrease in convergence. For this reason and after the iterative and block-iterative solvers proved to have convergence difficulties, the direct solver was used. Since convergence to the analytical solution is not ensured by the direct solver, a convergence study was performed for different optimised geometries by altering the number of B-spline subdivisions and comparing to low-order results. Based on these results, to achieve a good trade-off between calculation accuracy and run time, two patches were defined one for the submerged surface (Patch 1) and one for the interior free surface (Patch 2), each with 13 subdivisions in the parametric direction u, and 3 subdivisions in the parametric direction v, following WAMITs definition of the parametric directions. A representation of a hull defined with this method is shown in Fig. 3, where the two patches and their defined parametric directions can be identified.

For all runs the irregular frequency removal option of WAMIT was used. This prevents the optimisation algorithm from converging on solutions that generate numerical errors due to irregular frequencies in WAMIT.

2.4. Method verification

The method in [15] was re-implemented and verified. In this process some extensions were found necessary for the optimisation problem to be robustly defined. An overview of the performed studies within this work to verify and expand the re-implemented method is provided in this and the following sub-sections. The main additional requirements discussed here are: (1) Additional constraints needed to be defined to ensure that the generated shapes were closed and not self-crossing. (2) A number of error checks needed to be introduced to avoid the optimisation from selecting shapes that generated numerical errors in the calculation of the hydrodynamic coefficients. These extensions were key in allowing for the investigation of the most suitable geometry definitions and optimisation algorithms, since with the more complex and adaptable geometry definition, these improved implementations

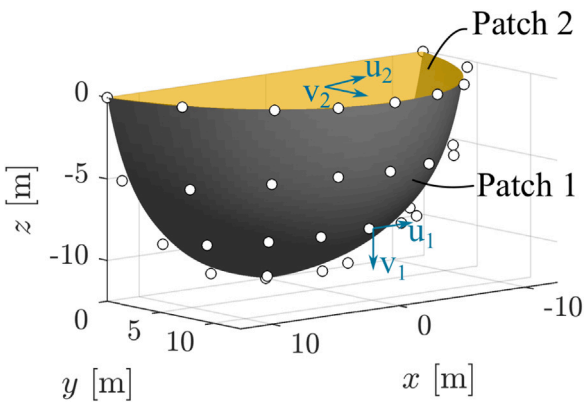

Fig. 3. Example hull geometry approximated with two B-spline surfaces, identified as Patch 1, and Patch 2. The parametric directions u and v as defined for each patch are also represented here [17].

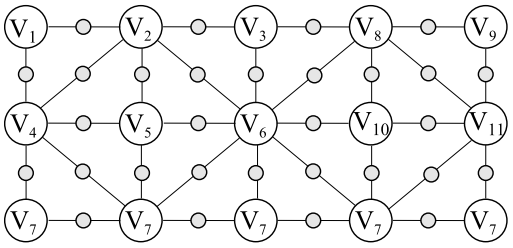

Fig. 4. Interpolation scheme for the generation of additional points for the B-spline approximation based on the polyhedron vertices [17], adapted from [14].

challenged the optimisation to search more of the design space. This improved search increased the probability of generating solutions that produced unexpected errors. Additionally, the enhanced method discussed here is applicable to any degree-of-freedom. In summary, these extensions increase the robustness of the optimisation approach, since they enable the application of the method to a much wider range of problems of WEC design optimisation.

With regards to the geometry definition, the interpolation strategy represented in Fig. 4 for a set of points had to be modified for the geometry to be closed. With reference to Fig. 2, the ϕ value of points interpolated between vertex V7, and the vertices V5, V6, V10 and V11 was not interpolated but the ϕ value of the latter vertices was adopted. For example, $\phi_{7-5} = \phi_5$. This is because ϕ_7 is defined to be zero. In the case of the point interpolated between vertex V7 and vertex V11, not doing the above results in a geometry that does not close, because the interpolated points do not lie on the symmetry plane.

To reproduce McCabe's results, first the power calculation was verified with one of the benchmark shapes described in [15], as well as one of the resulting optimal geometries. The optimal geometry resulting from power maximisation in the case of a maximal power restriction on the PTO of 5 MW and a maximal stroke of 5 m (see Figure 3 and associated text in [15]) approaches a hemispherical shape. The power calculation results show good agreement with McCabe's results with a percentage difference of around 6.3%. To understand the source of the variation, a study was performed here to obtain the percentage deviation due to the use of random phase shifts for the superposition of the spectral components of the waves. The percentage deviation due to varying phase shifts in each power calculation was found to be only 0.1–0.2%. Additionally, the error introduced by eliminating frequencies between 3 and 4 rad/s in the spectrum representation, which were considered in [15], and using a step size of 0.2s instead of 0.05s was studied. This was found to result in a difference in the calculated power of only 0.14%. According to these results, the average power

is underestimated in comparison to McCabe's results with a percentage difference of 6%. This is considered an acceptable difference, which can stem from differences in the numerical implementation, such as the WAMIT set-up, including the choice of solver and the resolution of the analysis, which was described in more detail in Section 2.3. The differences can also originate in the implementation of the power calculation, such as in the choice of the time step size for the evaluation of the instantaneous power. This is mentioned in [19].

After verification of the geometry definition and the power calculation, the optimisation process was tested for the three objective functions described in [15]. It was found that a number of extensions were necessary to ensure a robust optimisation set-up, which are detailed in the following section. Through a new verification of the optimisation process, it was proven that the introduced extensions did not affect the ability of the optimisation process to converge into the same type of optimal solutions as before the extension. The obtained mean annual power values with objective function $-\bar{P}/V$ were, however, only about 60% of the values obtained by McCabe. Although this cannot be concluded from the work presented in [15], this could be due to the shapes obtained by McCabe being self-crossing and generating numerical errors in WAMIT, which resulted in erroneously high mean annual power values.

2.5. Method extensions

The required extensions to the method, as detailed in [15], are presented here.

2.5.1. Geometry definition

It was found that the definition of the geometry was not robust enough, and that self-crossing geometries could result if no further constraints were defined. An example of such self-crossing geometries is shown in Fig. 5. To avoid self-crossing geometries from being generated in the optimisation process, the range of ϕ_n for $n = 2, 5, 8, 10$ was constrained. This was done so that vertices V2 and V5 were always in octant 'V (+x +y −z)', and V8 and V10 in octant 'VI (−x +y −z)':

$$\frac{\pi}{16} \leq \phi_n \leq \pi/2 \quad \text{for} \quad n = 2, 5$$
$$\frac{\pi}{2} \leq \phi_n \leq 15\pi/16 \quad \text{for} \quad n = 8, 10$$

2.5.2. Numerical errors

Some geometries caused numerical errors in the estimation of the hydrodynamic coefficients in WAMIT, which can missguide the optimisation search. To avoid this from happening, multiple checks were introduced after the hydrodynamic coefficient calculation, so that shapes generating these errors are penalised and no objective function evaluation is performed for them. The error checks were implemented so that they should detect any faults in the geometry evaluation without unnecessarily reducing the feasible solution space. It was also necessary to keep the process computationally efficient. Defective geometries were identified and not evaluated. Various implementations and thresholds were tested to ensure their effectiveness. This was done by (1) applying the different implementations to preliminary optimisation results, and (2) running the optimisation with the various implementations that proved to work in the first step. The numerical checks introduced in the following paragraphs were found to give the best trade-off in the fulfilment of these requirements.

A first check for WAMIT convergence consists in comparing the displaced volume calculated automatically by WAMIT using three separate approaches. For this reason, the three values of the volume are compared in the first instance. If any of the three volumes differs by more than 2% from their mean value, the geometry is penalised by setting $\bar{P} = 0$, $V = \text{Inf}$ and $S = \text{Inf}$.

For certain shapes and numbers of patch subdivisions for the calculation of the velocity potential, some diagonal terms of the damping coefficient matrix attained negative values at some frequencies. This could result in an erroneous power calculation or could be indicative of non-converged results for the hydrodynamic coefficients. To avoid the selection of geometries resulting in erroneously high power values, the lowest value of the added damping coefficient over all frequencies $C_{a,MIN} = \min(C_a(\omega))$ is evaluated in relation to the highest value $C_{a,MAX} = \max(C_a(\omega))$. This is done for each diagonal term (i.e. degree of freedom) separately. If the value is sufficiently negative ($C_{a,MIN} < 0$ and $|C_{a,MIN}| > C_{a,MAX} \cdot 10^{-2}$), the geometry is penalised. If, however, the value is small and negative ($C_{a,MIN} < 0$ and $|C_{a,MIN}| \leq C_{a,MAX} \cdot 10^{-2}$), diagonal added damping coefficient values for each frequency are evaluated and if they are negative they are set to zero.

A specific combination of vertices can also result in numerical errors in WAMIT. To be able to identify these combinations and discard the associated geometries, the following approach was taken. Firstly, the Degrees of Freedom (DoFs) at which the highest $M_{a,MIN}/M_{a,MAX}$ and $C_{a,MIN}/C_{a,MAX}$ ratios occur are identified as $\text{DoF}_{M_{a,MAX}}$ and $\text{DoF}_{C_{a,MAX}}$, respectively. The frequencies at which these occur are also established $\omega_{M_{a,DOFMAX}}$ and $\omega_{C_{a,DOFMAX}}$. Then the coordinates of the vertices describing the geometry are varied slightly (by multiplying them with 1.0001). At the previously identified DoFs and frequencies, the maximal values of the added mass ($M_{a,DOFMAX}$) and added damping ($C_{a,DOFMAX}$) coefficients are compared to equivalent coefficient values obtained for the sightly varied geometry ($M_{a,check}$ and $C_{a,check}$). If the difference between $M_{a,check}$ and $M_{a,DOFMAX}$, or $C_{a,check}$ and $C_{a,DOFMAX}$ is greater than $0.1 \cdot M_{a,DOFMAX}$ or $0.1 \cdot C_{a,DOFMAX}$, respectively, the geometry is penalised and the objective function is not evaluated.

For some geometries, despite having positive added damping values, the hydrodynamic coefficients varied so widely when analysed with different numbers of B-spline subdivisions, that the calculated average power showed large fluctuations. In some other cases, WAMIT happened to run with a set number of subdivisions, but did not run for many of the other combinations. Since WAMIT convergence cannot be proven in these cases, geometries exhibiting this type of behaviour should not be considered. With this purpose, two additional resolutions ((14,14,4,4) and (12,12,4,4)) for the WAMIT solution were used, and if any of the mentioned issues were encountered in both cases, geometries were penalised and not evaluated further. The resolutions are denoted by 'the number of knot spans in u-direction for patch 1, the number of knot spans in u-direction for patch 2, the number of knot spans in v-direction for patch 1, and the number of knot spans in v-direction for patch 2'.

3. Case studies

In this section, the studied cases and approaches employed to investigate the most suitable choice of optimisation algorithm and geometry definition for WEC geometry optimisation are introduced. The objective functions used to study both choices are introduced first. Then the approach to find the most suitable optimisation algorithm is presented. The most suitable optimisation algorithms were then used to identify the most suitable geometry definition. Small modifications to the most suitable optimisation algorithms had to be considered for the different geometry definitions, which are also reported here.

3.1. Geometry evaluation according to the objective function

Multiple metrics have been analysed on their suitability for comparison of WECs [32,33], where the Levelised Cost of Energy represents the ultimate metric for this purpose, because it depicts the price of energy generation for a certain technology. However, this is very difficult to quantify reliably due to lack of data and experience at initial stages of a WEC design process. For this reason, alternative metrics have been previously used for WEC comparison, such as, mean annual power and annual energy production [7,24], Capture Width (CW) [34] or Capture Width Ratio (CWR) [35–37]. Although when compared to CW,

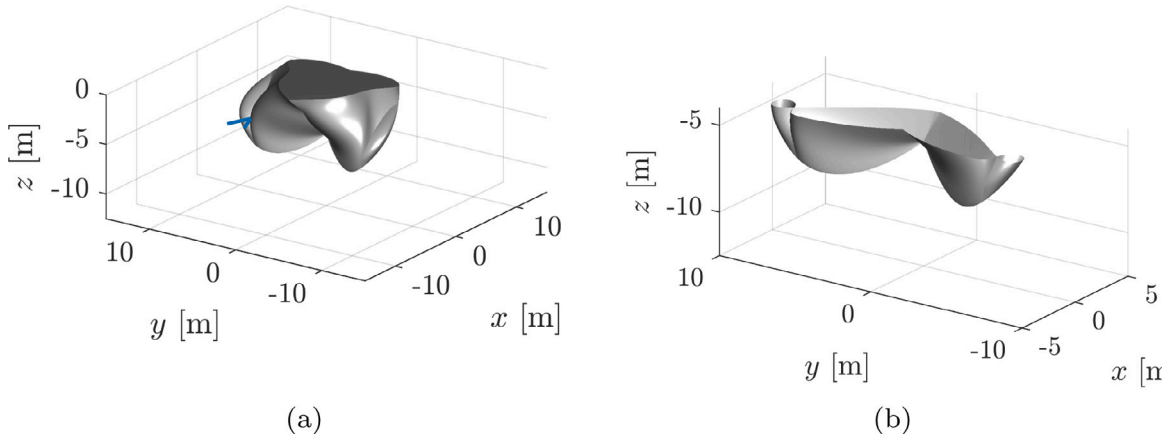

Fig. 5. Example of a self-crossing geometry resulting from an optimisation with the re-implemented method with objective function $-\bar{P}/V$. (a) Complete submerged hull. The blue arrow indicates wave direction [17]. (b) Hull cut at z = −4 m [17].

CWR takes into consideration device size in the objective function, and this avoids the optimisation from converging on very big devices, the definition of a characteristic length for different types of devices is not straightforward. A few different metrics are selected here to assess how optimal geometries vary depending on the selected metric and on the choice of the device's characteristic size. In this way, their suitability as the objective function of a WEC optimisation process can be assessed. An overview is given below, where $\bar{P}$ represents the mean annual power, V the submerged volume, and S the submerged surface area. $\bar{P}$ is calculated here for a site off the West-Shetland shelf employing the scatter diagram in [15].

The annual average power and the displaced volume V were employed in the objective functions of the original implementation [15], where the volume's cubic root was used as a proxy for a characteristic length. The following objective functions are, therefore, minimised in the optimisation process:

$$f_1 = -\bar{P} = f(x_1, x_2, \dots, x_{22}), \tag{2}$$

$$f_2 = -\frac{\bar{P}}{\sqrt[3]{V}} = f(x_1, x_2, \dots, x_{22}), \tag{3}$$

$$f_3 = -\frac{\bar{P}}{V} = f(x_1, x_2, \dots, x_{22}), \tag{4}$$

New objective functions are introduced based on the actual submerged surface area S, where its square root is also used as a proxy for a characteristic length, and the displaced volume raised to the power of 2/3 is used as a proxy for the submerged surface area. These objective functions are also set to be minimised within the optimisation process.

$$f_4 = -\frac{\bar{P}}{V^{2/3}} = f(x_1, x_2, \dots, x_{22}) \tag{5}$$

$$f_5 = -\frac{\bar{P}}{S} = f(x_1, x_2, \dots, x_{22}) \tag{6}$$

$$f_6 = -\frac{\bar{P}}{\sqrt{S}} = f(x_1, x_2, \dots, x_{22}) \tag{7}$$

3.2. Optimisation algorithms

Different optimisation algorithms can be more suitable for different types of problems, and their set-up and parameter tuning will have an effect on their efficiency and effectiveness. Meta-heuristic methods are more suitable to solve complex problems with many optimisation variables, since they are generally able to find a good enough solution within an acceptable time scale, whereas the computational time required with exact methods increases rapidly with problem complexity [25]. For this reason, two meta-heuristic optimisation algorithms are applied to this study, particle swarm optimisation and genetic algorithms. Each of these algorithms is implemented with various setting variations to be able to identify the better performing combination of parameter values.

Table 1
Overview of GA implementations based on different parameter combinations.

Implem.	N_{Ind}	$N_{Parents}$	$N_{Pairings}$	N_{Elite}
I [15]	22	10	2	2
II	22	20	1	2
III	44	42	1	2
IV	44	40	1	4
V	22	20	2	2

To find an implementation that is capable of achieving better results with less function evaluations, a different approach than presented in Section 2.2 as used by McCabe is applied here. The optimisation process is iterated until a maximum number of generations (MaxGen= 100) is reached, after which it is hoped that the genetic algorithm will converge on a relatively optimal WEC shape. Additionally, another termination criterion was introduced, so that if the objective function integer, calculated in [W] and [m], does not improve over 20 generations after a minimum of 50 generations, the optimisation is considered to have converged.

Genetic algorithm

Genetic Algorithms (GAs) were introduced in Section 2.2 with the re-implemented method. Genetic algorithms are implemented based on the GA Toolbox from the University of Sheffield [38]. The considered parameter variations are listed in Table 1.

Particle swarm algorithm

Particle Swarm Optimisation (PSO) is based on the behaviour of bird flocking and fish schooling, where solutions of the optimisation problem are represented by particles moving in space. The position of a particle i is described by vector $x_i \in \mathbb{R}^n$ and its movement by vector $v_i \in \mathbb{R}^n$. In each optimisation step t each particle changes its position and velocity based on: its previous position $x_i(t-1)$ and velocity $v_i(t-1)$; its best previous position p_i; and the best position found in the swarm so far p_g according to Eqs. (8) and (9), where a weighting of the particle's inertia through an inertia factor φ_{ic} is included.

$$x_i(t) = x_i(t-1) + v_i(t). \tag{8}$$

$$\begin{aligned} v_i(t) = &\varphi_{ic} \cdot v_i(t-1) + \varphi_1 \cdot rand_1 \cdot (p_i - x_i(t-1)) \\ &+ \varphi_2 \cdot rand_2 \cdot (p_g - x_i(t-1)). \end{aligned} \tag{9}$$

Table 2
Overview of PSO implementations based on different parameter combinations.

Implem.	N_{Ind}	φ_{ic}	φ_1	φ_2	φ	Constraint
I	22	#1	0.5	1.25	1.75	'absorb'
II	44	#1	0.5	1.25	1.75	'absorb'
III	66	#1	0.5	1.25	1.75	'absorb'
IV	22	#1	0.5	1.25	1.75	'reflect'
V	22	#1	1.25	0.5	1.75	'absorb'
VI	22	#1	0.5	0.5	1	'absorb'
VII	22	#1	1.25	1.25	2.5	'absorb'
VIII	22	#1	2	2	4	'absorb'
IX	22	#2	0.5	1.25	1.75	'absorb'

Acceleration constants control the weight of the local and global best values in the update formula. Limits for the sum of these parameters were defined following the recommendations by Perez et al. [39] to ensure stability of the algorithm.

$$0 < \varphi = \varphi_1 + \varphi_2 < 4 \tag{10}$$

The inertia factor is defined as in Eq. (11), so that it increases in each generation (Gen) [39]. This is because it is assumed that towards the end of the optimisation process less exploration of the solution space will be required and the solutions will be already converging towards an optimum, around which more exploitation will be beneficial.

$$\varphi_{ic} = \varphi_{ic,high} - \varphi_{ic,low} * (\text{Gen} - 1)/(\text{MaxGen} - 1). \tag{11}$$

Two options for the calculation of the inertia lower and upper limits are used. In option #1 the limits are fixed following the recommendation in [40] with:

$$\varphi_{ic,upper} = 0.9; \qquad \varphi_{ic,lower} = 0.4.$$

In option #2 the limits are defined based on the attraction factors φ_1 and φ_2 following the recommendation in [39]

$$\varphi_{ic,lower} = (\varphi_1 \cdot \varphi_2)/2 - 1; \qquad \varphi_{ic,upper} = \max(0.9, \varphi_{ic,lower}).$$

How constraint variations are dealt with can be defined in different ways. Here two options are considered: 'absorb', where the velocity is set to 0, and 'reflect', where the velocity is set to the negative of the current velocity. In both cases, the optimisation variable exceeding the bounds is set equal to the exceeded bound.

The implementation of this algorithm is based on the code given in [41]. This implementation uses a global best topology, and includes an inertia weight in the update function. The considered parameter variations are listed in Table 2.

Performance indicators

To evaluate the performance of a single-objective optimisation algorithm different indicators can be used. Because of the stochastic nature of most meta-heuristic algorithms, multiple runs of the same algorithm are required to estimate their performance. Each case is run three times, to allow for a fairer comparison of the algorithm performance. For context, when new algorithms are introduced it is common practice to repeat runs around 100 times for a fair algorithm comparison. In this case, proven algorithm implementations are applied, so that the use of three repetitions is considered sufficient to be able to recognise advantageous and disadvantageous trends of the different implementations. Once advantageous trends have been recognised, further repetitions of the better performing algorithm implementations could be carried out for more detailed comparison.

According to [42], the metrics commonly used as indicators for algorithm performance are:

- **Mean Best Fitness** (MBF)
  MBF is used to measure the effectiveness or solution quality of the algorithm. It employs the average of the best objective function value at the end of the optimisation run for multiple runs of the same algorithm set-up.
- **Average number of Evaluations to a Solution** (AES)
  AES is a measure for algorithm efficiency or speed, independent from the used hardware. Given that the required result of the search is known, the number of function evaluations until the successful solution has been found is used. This value is averaged over a set of successful runs.
- **Success Rate** (SR)
  SR is a measure for the robustness of the algorithm. It can be calculated as the percentage of runs that find a solution of the required quality. This is applicable to cases where the optimal solution can be identified or a criterion such as a threshold describing sufficient quality of the solution can be defined.

Since the optimal solution is not known, instead of the Average number of Evaluations to a Solution (AES), the averaged best objective function value is plotted here against the number of function evaluations as an indicator of the algorithm efficiency. With the same reasoning, the Success Rate (SR) cannot be quantified. For this reason, a threshold for each objective function is defined, to identify successful solutions. For the objective functions used by McCabe, the best objective function values achieved in the runs using his optimisation algorithm set-up with the extended implementation of the method are used as thresholds. For the other cases, a 5% deviation of the best objective value achieved over all runs is used as the threshold value. In both cases, these are referred to as the 'Threshold' in the results. When comparing with McCabe's results (indicated as 'McCabe' in the results), as well as with the results from the extended method, it should be considered that, due to the optimisation set-up, those final objective function values were achieved after 5010 function evaluations. The Mean Best Fitness (MBF) is calculated from the best objective function values at the end of the optimisation process. For both the AES equivalent and MBF, the absolute values of the objective function results are used in the discussion of the results, since they were just set to be negative so that the optimisation is formulated as a minimisation problem.

3.3. Geometry definition

Four different geometry definitions are used, to identify their limitations and suitability for different problems. These are represented in Fig. 6, with two axisymmetric floaters: (a) a hemisphere, and (b) a vertical cylinder; and two x−z plane symmetric bodies: (c) a barge and (d) a B-spline surface approximating vertices of a polyhedron as in [15]. For an equitable comparison between the different cases, the variable bounds used for the simple shapes are comparable to those used for the B-spline approach, and are summarised in Table 3.

The most suitable optimisation algorithms found for each case were applied when investigating the suitability of the geometry definitions. Due to the lower number of decision variables some of the algorithm parameters needed to be adjusted.

The adapted PSO implementations vary only in the number of variables and individuals, but in the case of the GA implementations, equivalent parameter definitions had to be defined, which are represented in Table 4. The number of individuals was taken as 12 for the cases where 22 individuals had been used before, and 24 for the cases where 44 individuals had been employed. This is to ensure a minimum number of individuals in the population, since one to three individuals (equalling the number of optimisation variables) would not be enough for a population based optimisation algorithm to function correctly.

Within the genetic algorithm implementations, the mutation rate cannot be defined as before in dependence of the number of variables and is defined instead through a constant rate of 3/11. In this way, in average the one (for the hemisphere) to the three (for the barge) genes have 3/11 probability of being mutated. This is, the mutation of one of the genes of three individuals out of 11 per generation can be expected for the one variable case, of one gene of six individuals for the two variable case, and of one gene of nine individuals for the three variable case.

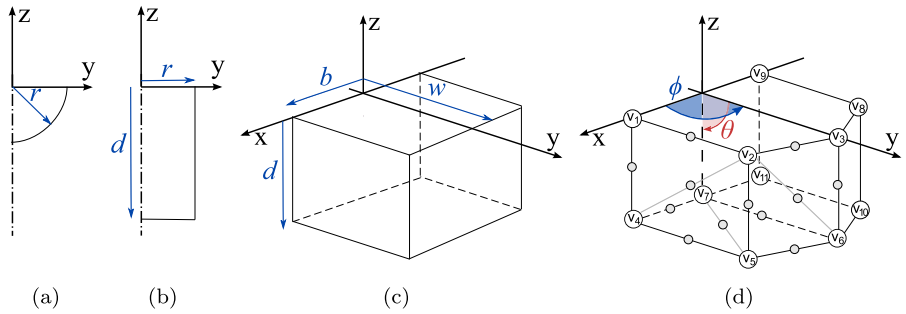

Fig. 6. Geometry definitions [17]: (a) Hemisphere, (b) Vertical cylinder, (c) Barge, (d) Polyhedron defining B-spline surface with numbered vertices and example representations of the interpolated points in grey (Adapted from Figure 1 in [15]). The x–z plane is assumed to be a symmetry plane.

Table 3
Overview of optimisation problem formulations using different geometry definitions.

Geometry definition	Decision variables	Variable bounds
a	r	$2.5\ \text{m} \le r \le 12.5\ \text{m}$
b	$r,\ d$	$2.5\ \text{m} \le r, d \le 12.5\ \text{m}$
c	$w,\ b,\ d$	$2.5\ \text{m} \le w, b, d \le 12.5\ \text{m}$
d [15]	22 coordinates	$2.5\ \text{m} \le r_n \le 12.5\ \text{m} \quad \vert\ n = 1, \ldots, 11$ $-7\pi/16 \le \theta_n \le -\pi/16 \quad \vert\ n = 4, 5, 6, 10, 11$ $\pi/16 \le \phi_n \le 15\pi/16 \quad \vert\ n = 2^{a},\ 3,\ 5^{a},\ 6,\ 8^{a},\ 10^{a}$

[a]More restrictive bounds were applied in these cases, see Section 2.2.

Table 4
Summary of GA equivalent implementations for simple shapes.

Implementation	N_{Ind}	$N_{Parents}$	N_{Pair}	N_{Elite}	MaxGen
GA-IV	24	20	1	4	70
GA-V	12	10	2	2	75

4. Results

4.1. Suitability of the optimisation algorithm

The previously introduced implementations of the genetic and particle swarm optimisation algorithms are applied to a single DoF (Surge) and a multi-DoF (Surge, Heave and Pitch) oscillating device using objective functions $\bar{P}$, $\frac{\bar{P}}{V^{\frac{1}{3}}}$, $\frac{\bar{P}}{V^{\frac{2}{3}}}$, $\frac{\bar{P}}{V}$, $\frac{\bar{P}}{S}$, and $\frac{\bar{P}}{S^{\frac{1}{2}}}$. A detailed discussion of the results is given here for two of the studied cases. These are used as examples to demonstrate the process for selection of the most suitable algorithms for each case. Results for the other cases can be found in the Appendix. All results are summarised at the end of this section in Table 8.

$\bar{P}/V$-Surge

The effectiveness and robustness of the algorithms are measured through the MBF and SR, respectively. The results of these indicators are summarised in Table A.12. The best performing algorithms in terms of MBF are PSO-II and PSO-III followed by PSO-VIII and GA-IV. The SR is relatively high for most algorithms, indicating that the chosen threshold value achieved with McCabe's optimisation algorithm set-up was rather low. This could be due to the optimisation set-up in [15] not being the most suitable for this optimisation problem.

Regarding the algorithms efficiency and speed, the averaged best objective function values per function evaluation are represented in Figs. 7(a) and (b) for the GA and PSO implementations, respectively. PSO-I and PSO-VII have the steepest improvement in objective function value in the first 500 function evaluations. After that, PSO-VIII takes over, approaching the optimal value faster than PSO-II and PSO-III. PSO-VIII has the same slope and objective function values as PSO-II around 1800 and 2200 function evaluations. However, the evaluation of PSO-VIII ends at this point, and PSO-II continues improving and reaches convergence around 3200 function evaluations. To investigate this behaviour further, PSO-VIII was run for further 50 generations. The implementation surpasses PSO-II after 2200 evaluations and then follows a similar trend achieving higher objective function values.

Table 5
Additional PSO implementation for a surging only case, minimising $-\bar{P}/V$.

Implementation	N_{Ind}	φ_{ic}	φ_1	φ_2	φ	Constraint
PSO-X	44	(a)	2	2	4	'absorb'

Overall, algorithms with a higher number of individuals (PSO-II, PSO-III and GA-IV) seem to have a performance advantage versus the other algorithms. However, no further improvement is achieved by increasing the number of individuals to three times the number of variables (PSO-III) instead of two times (PSO-II). Additionally, high acceleration constant values, seem to allow for a quicker search of the optimisation space than the increased number of individuals. In summary, the most suitable optimisation algorithms for the optimisation of a single-body oscillating in one DoF aiming at maximising the ratio of mean power to submerged volume are PSO-VIII followed by PSO-II. GAs seem to have a slower convergence in this case.

Due to the rapid initial improvement in objective function achieved by PSO-VIII, and the later similar behaviour of PSO-II, a combination of the beneficial characteristics of these two implementations was studied. For this reason, an implementation (PSO-X) with the following characteristics was evaluated for 50 and 75 generations in Table 5.

The MBF achieved with this combined algorithm is of 749.102 W/m^3 with a success rate of three out of three runs achieving the threshold value if run for 50 generations and of 783.881 W/m^3 with an SR of 100% if run for 75 generations. According to Fig. 7(b), a faster initial progression is achieved, but a similar behaviour to PSO-VIII can be observed after 1000 function evaluations. Overall, PSO-VIII run for 150 generations still showed the best results.

$\bar{P}/V$-Surge, heave and pitch

In the multimodal case, the highest MBF is achieved by PSO-II, which also achieves this value consistently with 100% success rate. This is shown in Table A.13.

In terms of convergence speed (see Figs. 7(c) and (d)), although algorithms such as PSO-VII and PSO-VIII show a faster improvement in the initial function evaluations, PSO-II takes over after 1000 function evaluations, and reaches convergence after 2000 function evaluations.

Overall, PSO-II shows the best performance. However, a combination of the characteristics of the PSO implementation VII and II was investigated to accelerate the initial improvement of PSO-II. For this reason, an implementation (PSO-X) with the following characteristics was studied in Table 6.

This new implementation has an MBF of 2704.970 W/m^3 and a success rate of one every three runs achieving the threshold value. It also does not seem to perform better in terms of speed. For this reason, PSO-II is finally selected as the most suitable algorithm for this case.

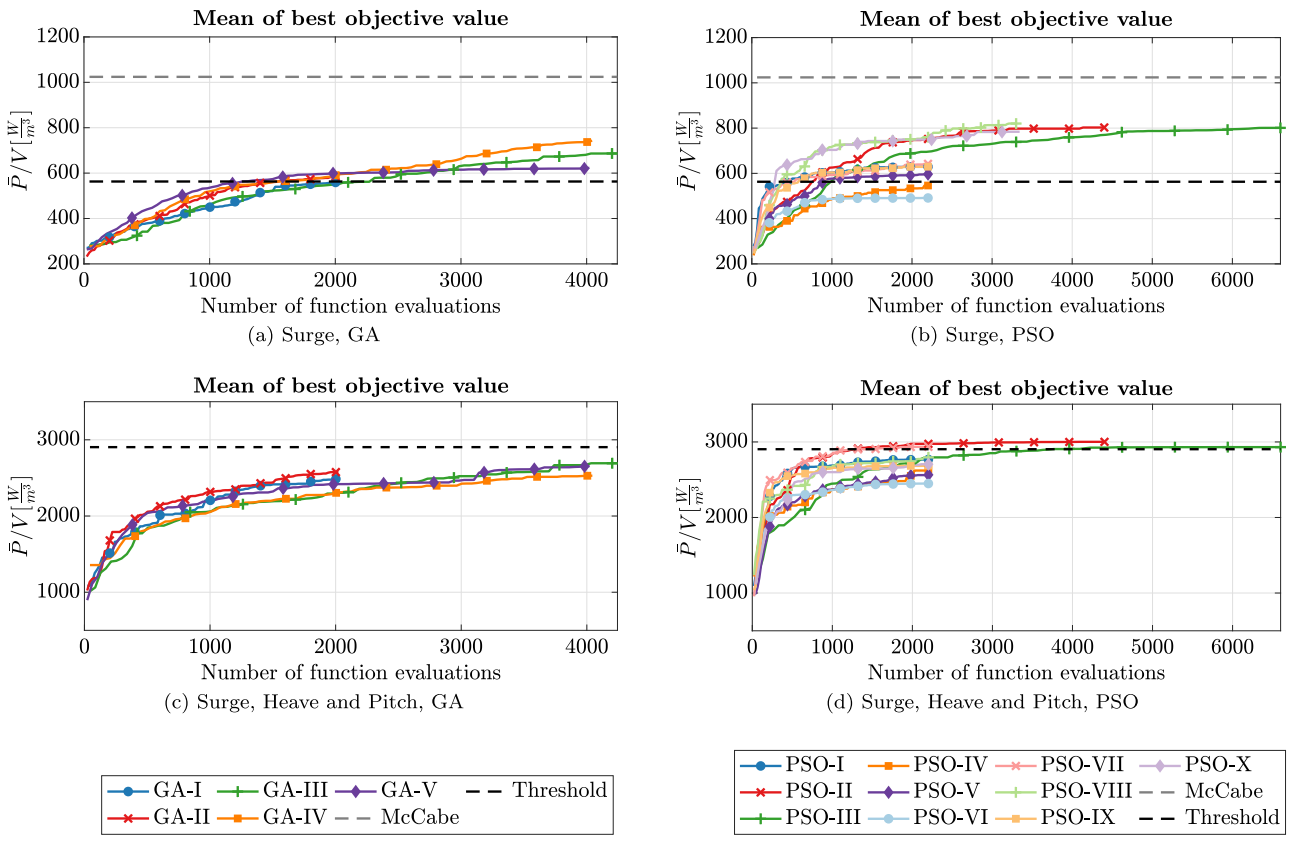

Fig. 7. Mean best objective value per number of function evaluations using $f_3 = -\bar{P}/V$ for a surging only device for (a) GA and (b) PSO implementations and for a device oscillating in surge, heave and pitch for (c) GA and (d) PSO implementations [17].

Table 6
Additional PSO implementation for a surging, heaving and pitching case, minimising $-\bar{P}/V$.

Implementation	N_{Ind}	φ_{ic}	φ_1	φ_2	φ	Constraint
PSO-X	44	(a)	1.25	1.25	2.5	'absorb'

Table 7
Additional PSO implementation for a surging only case, minimising $-\bar{P}/V^{2/3}$.

Implementation	N_{Ind}	φ_{ic}	φ_1	φ_2	φ	Constraint
PSO-X	66	(a)	1.25	0.5	1.75	'absorb'

Other cases

In all other cases, the most suitable algorithms were chosen following the same logic as introduced above based on the obtained results. The results for each of the studied cases are provided in the appendix for completeness. The most suitable optimisation algorithms for each case are summarised in Table 8.

As discussed above, some additional implementations were tested after analysis of the results, to ensure that the most suitable implementation for each case was found. This was only necessary in one additional situation. That is, when using objective function $\bar{P}/V^{2/3}$ for a surging only device, a further implementation was studied to better understand the effects of each of the parameters. Although it was found that PSO-III showed the best performance, the combination of PSO-III with an implementation showing a faster initial convergence such as PSO-V was investigated. An implementation (PSO-X) with the following combined characteristics was considered in Table 7.

Summary

The most suitable algorithms found for each of the studied cases are summarised in Table 8.

In optimisation approaches using objective functions f_1 and f_5, most algorithms converged into similar solutions. This could be an indicator of the optimisation problem being less complex. In these cases, GA's seemed to have a slight advantage over PSO implementations, where the generation of larger numbers of children seemed beneficial, exploring the solution space around the known solutions. In the multiple-DoF case utilising f_5, a PSO implementation showed better suitability, where a higher weight towards the global best solution was beneficial.

On the contrary f_4 showed the largest spread of solution quality depending on the used algorithm, which could be an indicator of the optimisation problem being more complex. In general, this seemed to be the case for the volume based objective functions f_2, f_3 and f_4, and for f_6 for which PSO implementations performed better than GA implementations. Implementations with a higher attraction towards the global best solution performed well in all cases except for the $f_4 = -\frac{\bar{P}}{V^{2/3}}$ multiple-DoF case, where bigger steps towards both the global and local best solutions were more advantageous. The latter was also beneficial for the single-DoF f_1, f_2 and f_3 cases, and for all f_6 cases. However, for the single-DoF case optimised for f_4, having a higher number of individuals proved advantageous. When these characteristics were combined for f_3, no improvement in the results was seen.

In general, the use of twice to three times the number of variables for the population size seemed to have a positive effect, although this did not consistently result in the best solutions. GA implementations with less than twice the number of variables for the population size did not perform well, and their use is, thus, discouraged. The application of the 'reflect' constraint handling option and of low acceleration constants, such as in PSO-VI, did not show any benefit, and are, therefore, not recommended.

Table 8
Summary of the most suitable optimisation algorithms for the studied cases.

Objective function	Surge	Surge, Heave and Pitch
$f_1 = -\bar{P}$	GA-IV	GA-V
$f_2 = -\frac{\bar{P}}{\sqrt[3]{V}}$	PSO-VIII	PSO-IX
$f_3 = -\frac{\bar{P}}{V}$	PSO-VIII	PSO-II
$f_4 = -\frac{\bar{P}}{V^{2/3}}$	PSO-III	PSO-VIII
$f_5 = -\frac{\bar{P}}{A}$	GA-IV	PSO-I
$f_6 = -\frac{\bar{P}}{\sqrt{A}}$	PSO-VIII	PSO-VIII

Table 9
Overview of optimisation problem results for various shape definitions for objective function $f_1 = -\bar{P}$. Previously obtained objective function values with B-spline surface definition are given for reference.

DoFs	Geometry definition	$\bar{P}$ [kW]	Variables [m]
Surge	with [15]	359.890	
	(a)	368.718	$r = 12.057$
	(b)	392.872	$r = 10.548$, $d = 11.443$
	(c)	413.524	$w = 7.718$, $b = 10.282$ $d = 12.496$
Surge, Heave and Pitch	with [15]	954.684	
	(a)	851.116	$r = 10.705$
	(b)	917.261	$r = 11.683$, $d = 9.328$
	(c)	954.068	$w = 6.930$, $b = 12.500$, $d = 11.544$

Table 10
Overview of optimisation problem results for various shape definitions for objective function $f_3 = -\bar{P}/V$. Previously obtained objective function values with B-spline surface definition are given for reference.

DoFs	Geometry definition	$\bar{P}/V$ [kW]	Variables [m]
Surge	with [15]	881.903	
	(a)	271.813	$r = 4.929$
	(b)	305.095	$r = 2.526$, $d = 12.500$
	(c)	313.536	$w = 2.500$, $b = 2.500$, $d = 10.003$
Surge, Heave and Pitch	with [15]	3056.609	
	(a)	1267.877	$r = 5.156$
	(b)	1140.612	$r = 5.319$, $d = 2.814$
	(c)	1295.417	$w = 12.500$, $b = 2.500$, $d = 2.500$

Table 11
Overview of optimisation problem results for various shape definitions for objective function $f_5 = -\bar{P}/A$. Previously obtained objective function values with B-spline surface definition are given for reference.

DoFs	Geometry definition	$\bar{P}/S$ [kW]	Variables [m]
Surge	with [15]	518.589	
	(a)	241.869	$r = 6.484$
	(b)	429.864	$r = 5.491$, $d = 6.657$
	(c)	410.237	$w = 3.626$, $b = 8.357$, $d = 9.237$
Surge, Heave and Pitch	with [15]	2875.168	
	(a)	1091.692	$r = 5.247$
	(b)	1557.632	$r = 5.276$, $d = 2.860$
	(c)	1276.621	$w = 2.500$, $b = 10.015$, $d = 2.500$

4.2. Suitability of the geometry definition

This evaluation is performed for a surging only device and a surging, heaving and pitching device for the same location off the Shetland shelf. The different geometry definitions are compared based on the achieved objective function values at the end of the optimisation process. For consistency with the previous sections, the absolute numbers of the objective function values are reported here. The optimisation results for $f_1 = -\bar{P}, f_3 = -\frac{\bar{P}}{V}$ and $f_5 = -\frac{\bar{P}}{S}$ are summarised in Tables 9, 10 and 11, respectively.

All simple shapes achieve higher mean annual power production values than the optimal shape using the B-spline definition (which follows from McCabe [15]) for the surging only case optimised to maximise the mean annual power. However, in the three DoF case, McCabe's shape definition achieves the highest value, although it performs very similarly to the optimal barge. It should be noted here that both the optimal cylinder's and the barge's volume approach the maximum set volume of 4000 m^3, whereas the shape defined through the B-spline surface has lower volumes of 3400 m^3 and 2260 m^3. Due to the other constraints imposed on the geometry (such as the upper bounds on the radii) it could be that constraints are more restrictive on volume for the designer-bias free shape than for the simple shapes.

When comparing the optimal results achieved with f_3, between 181% and 224% higher absolute objective function values are achieved with McCabe's shape definition for the single-DoF case, and between 136% and 141% higher absolute objective function values for the multiple-DoF case.

Analogously, higher absolute objective function values are achieved for f_5 with between 20% and 114% higher absolute objective function values for the single-DoF case, and between 121% and 152% higher absolute objective function values achieved for the multiple-DoF case.

Overall, the more adaptable shape definition implemented here generally obtains more suitable shapes for optimisation problems, where the objective function accounts for costs, or where more than one DoF of oscillation is considered.

5. Conclusions

The method for wave energy converter geometry optimisation presented by McCabe [15] was re-implemented and extended for robustness. The key elements of such an optimisation process were identified (the geometry definition, the objective function, the optimisation algorithm and the formulation of the optimisation problem) and a set of alternatives for each of the elements was defined. Here the suitability of the geometry definition and of the optimisation algorithm were studied by comparing results for a 1 Degree-of-Freedom (DoF) oscillating device and a 3 DoF case. In addition, six different objective functions were considered which used the ratio of the mean annual power to cost proxies based on the submerged volume or the submerged surface area.

A difference in the complexity of the solution spaces was identified in relation to the employed objective function. The solution space seems to be less complex for objective functions $f_1 = -\bar{P}$, and $f_5 = -\frac{\bar{P}}{S}$, where most algorithms tend to quickly converge on similar solutions. The solution space seems to be more complex for submerged volume based objective functions $f_2 = -\frac{\bar{P}}{\sqrt[3]{V}}, f_3 = -\frac{\bar{P}}{V}$ and $f_4 = -\frac{\bar{P}}{V^{2/3}}$, where algorithms show a diverse behaviour and more convergence difficulty. In the former case, genetic algorithm implementations are preferred, where higher numbers of children per generation appear to be advantageous. In the latter case, particle swarm optimisation implementations performed better, where an advantage was found in the use of higher acceleration constants and higher numbers of individuals in the population. A preferred algorithm for each combination of objective function and DoFs was found, with improvements in objective function values compared to McCabe's results of up to 11% while reducing the number of function evaluations and, hence, computation time up to about 50% of the original implementation's values. The use of the most suitable implementation for each case as found here is recommended.

The most suitable algorithms were then adapted and applied to simpler geometry definitions: a hemisphere, a vertical cylinder and a barge. Overall, the adapted version of McCabe's shape definition procedure obtained better performing geometries when the objective function accounted for costs, with up to 224% higher absolute objective function values achieved with this more complicated and adaptable shape definition.

For future wave energy converter geometry optimisation studies, the authors recommend the use of adaptable geometry definitions, such

as suggested by McCabe, due to their potential to find better trade-offs of performance and costs. Further improvements or analysis of McCabe's shape definition that could be considered in the future are, (1) ensuring a smooth transition at the symmetry plane, by enforcing the splines to be perpendicular to the symmetry plane at their crossing points and (2) considering different radius and volume constraints.

The results found in the present study define the most suitable methods for two of the key elements of a wave energy converter hull geometry optimisation. These results are a stepping stone towards the definition of a flexible and comprehensive method for hull geometry optimisation to aid device design for technology developers. The study of the most suitable methods for wave energy converter device comparison can also serve funding bodies to assess different technologies.

In a further study, the authors will compare the results from single-objective and multi-objective optimisation algorithms. This study was performed in order to establish the suitability of the objective functions and to determine the best formulation for the optimisation problems.

CRediT authorship contribution statement

Anna Garcia-Teruel: Conceptualization, Methodology, Software, Validation, Investigation, Visualization, Writing - original draft, Funding acquisition. **Bryony DuPont:** Supervision, Writing - review & editing. **David I.M. Forehand:** Conceptualization, Supervision, Writing - review & editing, Funding acquisition.

Declaration of competing interest

The authors declare that they have no known competing financial interests or personal relationships that could have appeared to influence the work reported in this paper.

Acknowledgements

The authors would like to thank the Energy Technology Partnership (ETP) and UKCMER (EPSRC, United Kingdom grants EP/I027912/1 and EP/P008682/1) for funding the Ph.D. project within which this work was performed. Additionally, we would like to acknowledge ETP PECRE for their funding support to make this research collaboration possible.

Appendix. Optimisation algorithm progress along the number of function evaluations, and MBF and SR values

See Figs. A.8–A.12 and Tables A.12–A.23.

Table A.12
Mean Best Fitness (MBF) and Success Rate (SR) for all algorithms applied to objective function $f_3 = -\bar{P}/V$ for a surging only device.

Algorithm	Implementation	MBF [W/m^3]	SR [–]
GA	I	559.603	2/3
	II	586.740	1/3
	III	686.580	3/3
	IV	742.797	3/3
	V	623.343	3/3
PSO	I	629.225	3/3
	II	802.664	3/3
	III	801.038	3/3
	IV	546.416	1/3
	V	596.608	2/3
	VI	491.306	0/3
	VII	642.171	2/3
	VIII	759.251 (820.155)[a]	3/3
	IX	629.388	2/3

[a]Note that the number in brackets is the value achieved when running this algorithm for 150 generations instead of 100 generations.

Table A.13
Mean Best Fitness (MBF) and Success Rate (SR) for all algorithms applied to objective function $f_3 = -\bar{P}/V$ for a surging, heaving and pitching device.

Algorithm	Implementation	MBF [W/m^3]	SR [–]
GA	I	2488.561	0/3
	II	2576.965	0/3
	III	2692.504	1/3
	IV	2528.971	0/3
	V	2654.185	0/3
PSO	I	2768.118	0/3
	II	3001.301	2/3
	III	2931.454	3/3
	IV	2638.838	0/3
	V	2564.598	0/3
	VI	2449.370	0/3
	VII	2936.040	2/3
	VIII	2795.731	1/3
	IX	2686.212	0/3

Table A.14
Mean Best Fitness (MBF) and Success Rate (SR) for all algorithms applied to objective function $f_1 = -\bar{P}$ for a surging only device.

Algorithm	Implementation	MBF [kW]	SR [–]
GA	I	356.663	0/3
	II	358.515	1/3
	III	360.992	2/3
	IV	361.725	2/3
	V	359.259	2/3
PSO	I	349.550	0/3
	II	355.532	1/3
	III	348.037	0/3
	IV	345.141	0/3
	V	351.985	0/3
	VI	350.634	0/3
	VII	351.723	1/3
	VIII	351.798	0/3
	IX	347.839	0/3

Table A.15
Mean Best Fitness (MBF) and Success Rate (SR) for all algorithms applied to objective function $f_1 = -\bar{P}$ for a device oscillating in surge, heave and pitch.

Algorithm	Implementation	MBF [kW]	SR [–]
GA	I	946.324	3/3
	II	948.775	3/3
	III	949.641	3/3
	IV	944.707	3/3
	V	951.860	3/3
PSO	I	945.930	3/3
	II	944.719	3/3
	III	945.649	3/3
	IV	931.182	3/3
	V	947.410	3/3
	VI	948.780	3/3
	VII	937.472	3/3
	VIII	936.870	3/3
	IX	938.881	3/3

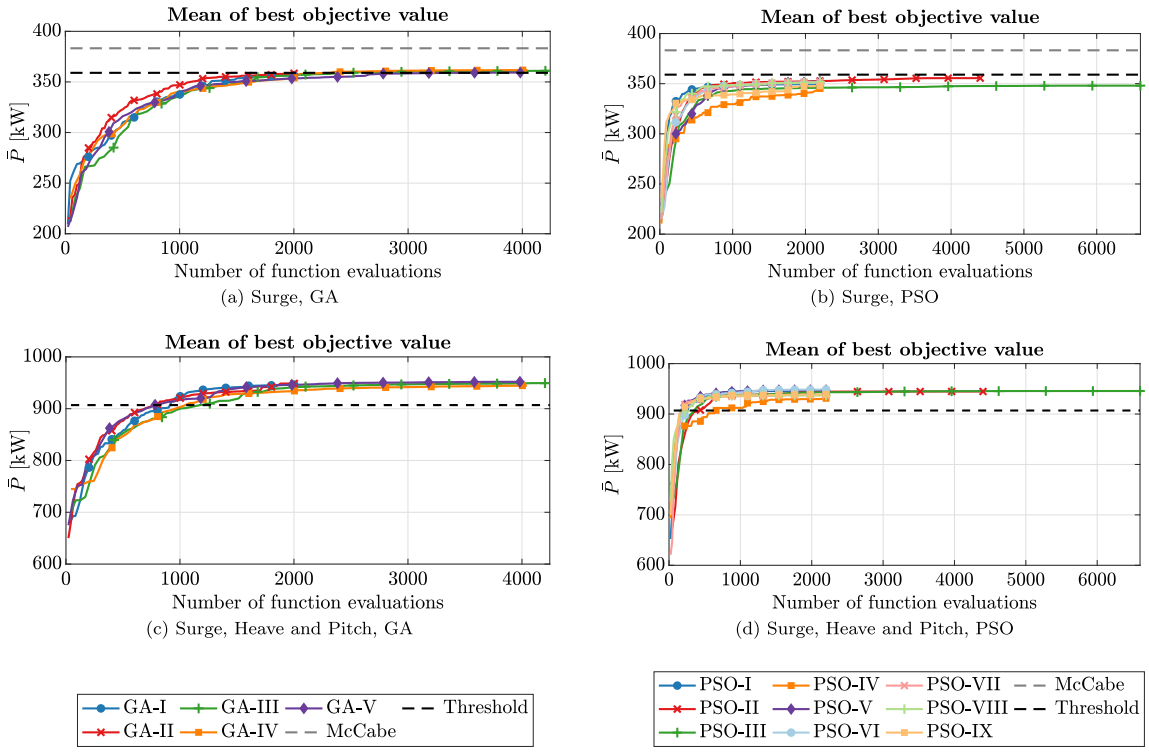

Fig. A.8. Mean best objective value per number of function evaluations using $f_1 = -\bar{P}$ for a surging only device for (a) GA and (b) PSO implementations and for a device oscillating in surge, heave and pitch for (c) GA and (d) PSO implementations [17].

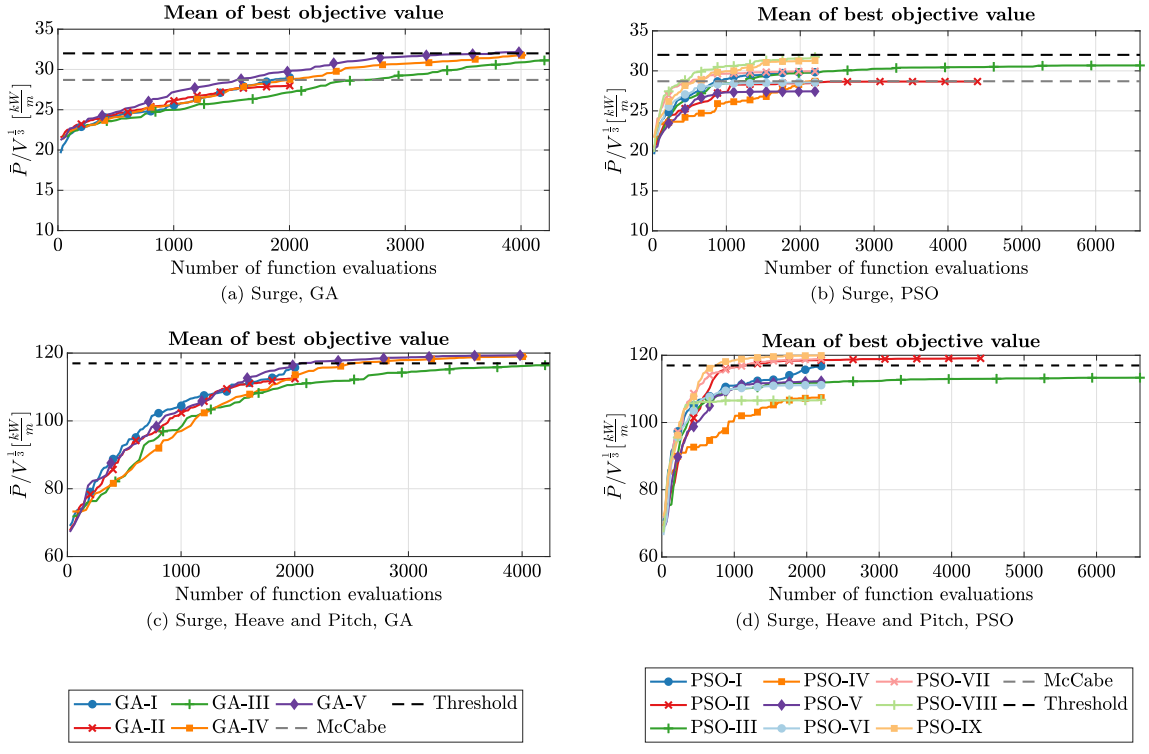

Fig. A.9. Mean best objective value per number of function evaluations using $f_2 = -\bar{P}/V^{\frac{1}{3}}$ for a surging only device for (a) GA and (b) PSO implementations and for a device oscillating in surge, heave and pitch for (c) GA and (d) PSO implementations [17].

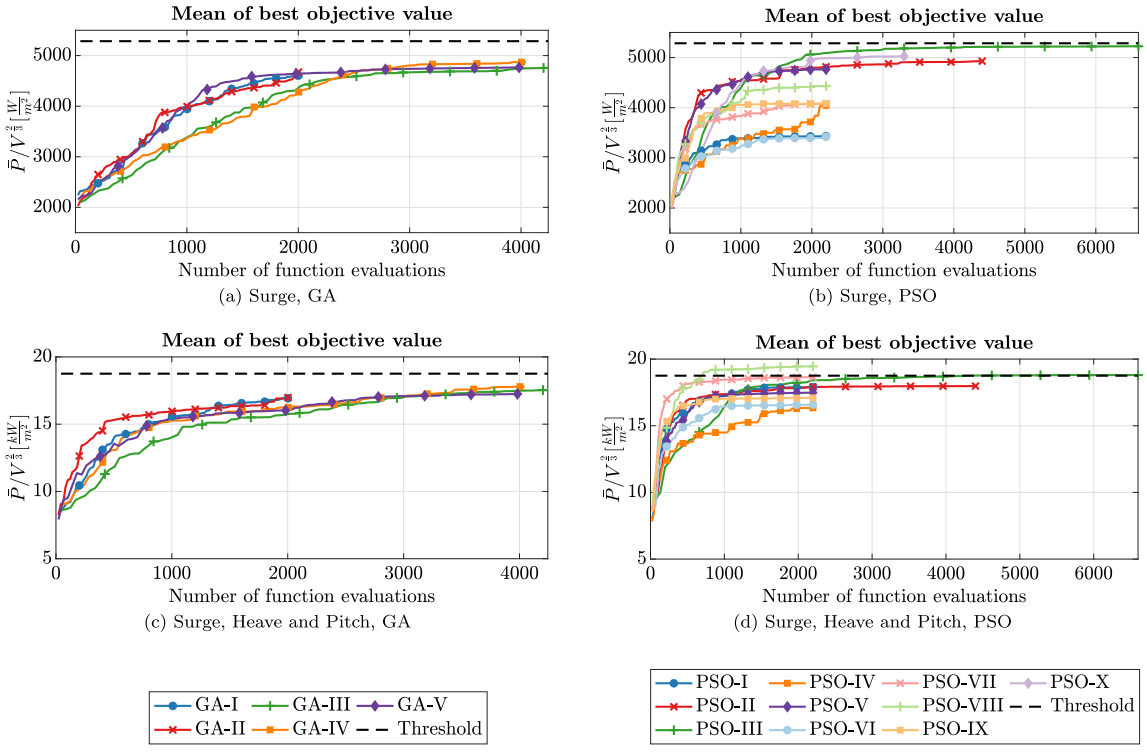

Fig. A.10. Mean best objective value per number of function evaluations using $f_4 = -\bar{P}/V^{\frac{2}{3}}$ for a surging only device for (a) GA and (b) PSO implementations and for a device oscillating in surge, heave and pitch for (c) GA and (d) PSO implementations [17].

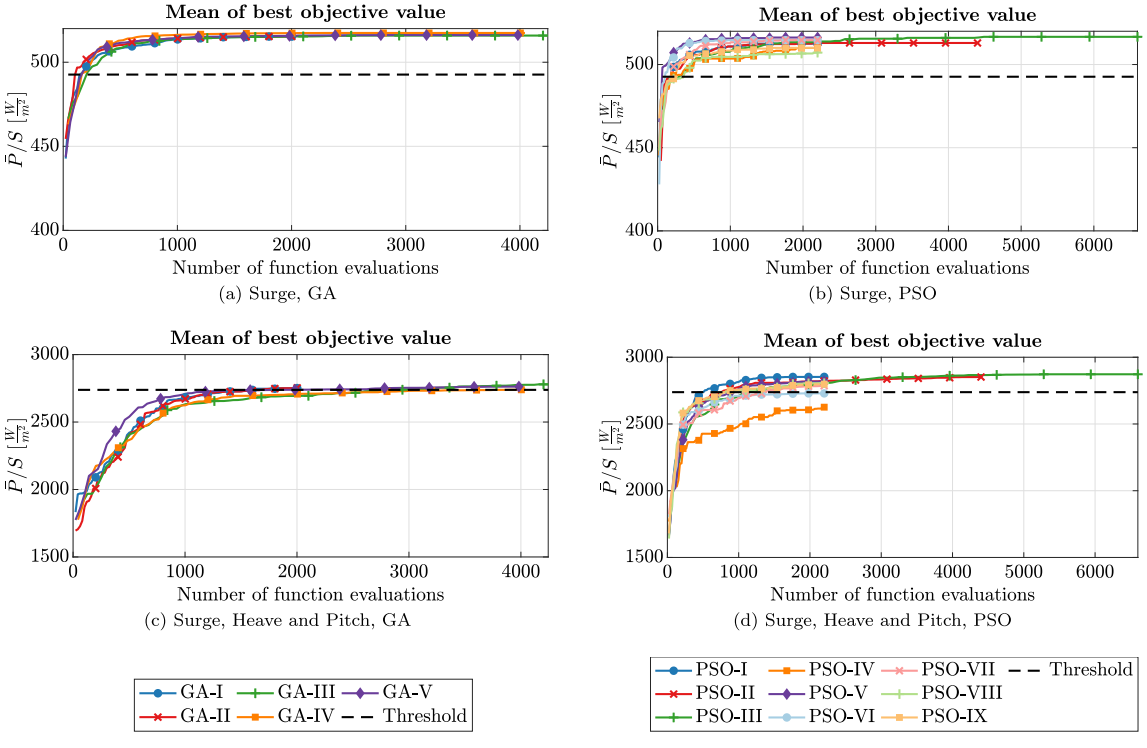

Fig. A.11. Mean best objective value per number of function evaluations using $f_5 = -\bar{P}/S$ for a surging only device for (a) GA and (b) PSO implementations and for a device oscillating in surge, heave and pitch for (c) GA and (d) PSO implementations [17].

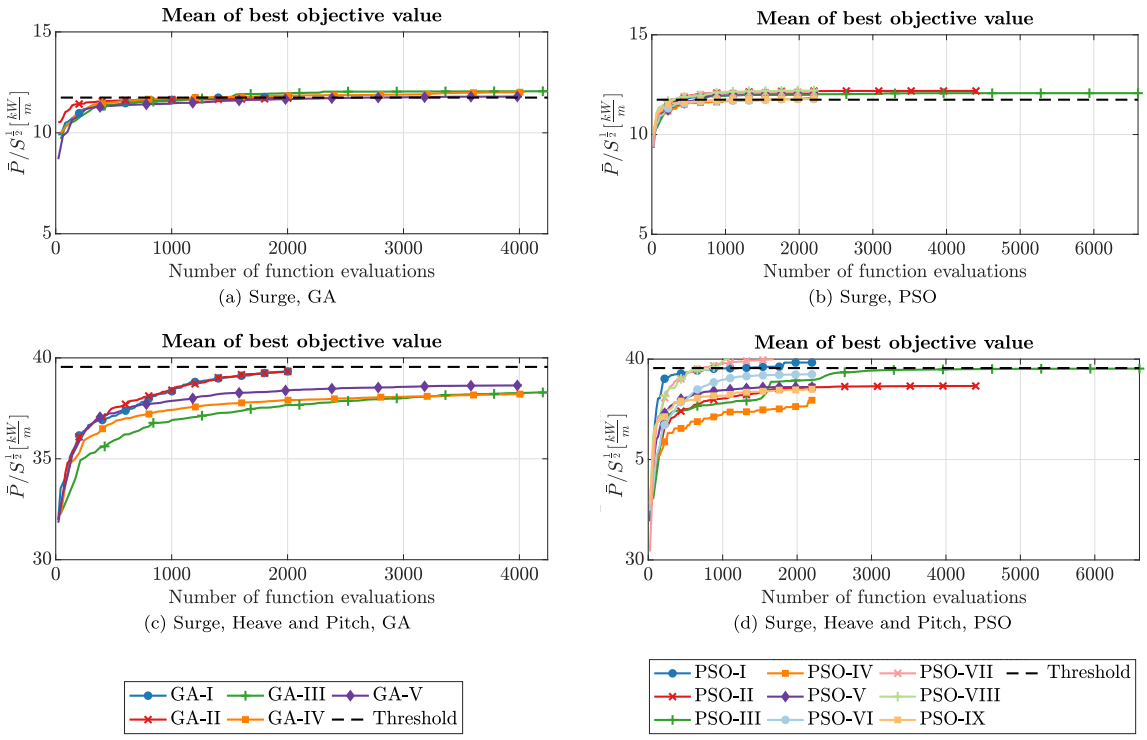

Fig. A.12. Mean best objective value per number of function evaluations using $f_6 = -\bar{P}/S^{\frac{1}{2}}$ for a surging only device for (a) GA and (b) PSO implementations and for a device oscillating in surge, heave and pitch for (c) GA and (d) PSO implementations [17].

Table A.16
Mean Best Fitness (MBF) and Success Rate (SR) for all algorithms applied to objective function $f_2 = -\bar{P}/V^{\frac{1}{3}}$ for a surging only device.

Algorithm	Implementation	MBF [kW/m]	SR [–]
GA	I	29.034	0/3
	II	27.996	0/3
	III	31.139	0/3
	IV	31.778	0/3
	V	32.151	2/3
PSO	I	29.832	0/3
	II	28.667	0/3
	III	30.678	1/3
	IV	28.704	0/3
	V	27.441	0/3
	VI	28.551	0/3
	VII	29.952	1/3
	VIII	31.726	2/3
	IX	31.288	1/3

Table A.17
Mean Best Fitness (MBF) and Success Rate (SR) for all algorithms applied to objective function $f_2 = -\bar{P}/V^{\frac{1}{3}}$ for a device oscillating in surge, heave and pitch.

Algorithm	Implementation	MBF [kW/m]	SR [–]
GA	I	115.820	1/3
	II	112.549	1/3
	III	116.437	1/3
	IV	119.007	3/3
	V	119.377	2/3
PSO	I	116.782	1/3
	II	119.091	2/3
	III	113.328	1/3
	IV	107.415	0/3
	V	112.271	2/3
	VI	111.111	1/3
	VII	118.903	2/3
	VIII	106.736	1/3
	IX	119.923	3/3

Table A.18
Mean Best Fitness (MBF) and Success Rate (SR) for all algorithms applied to objective function $f_4 = -\bar{P}/V^{\frac{2}{3}}$ for a surging only device.

Algorithm	Implementation	MBF [W/m^2]	SR [–]
GA	I	4603.590	0/3
	II	4674.434	0/3
	III	4757.015	0/3
	IV	4872.999	0/3
	V	4766.316	0/3
PSO	I	3431.302	0/3
	II	4928.454	0/3
	III	5225.255	1/3
	IV	4045.098	0/3
	V	4765.205	0/3
	VI	3417.741	0/3
	VII	4079.769	0/3
	VIII	4429.795	0/3
	IX	4079.888	0/3

Table A.19
Mean Best Fitness (MBF) and Success Rate (SR) for all algorithms applied to objective function $f_4 = -\bar{P}/V^{\frac{2}{3}}$ for a device oscillating in surge, heave and pitch.

Algorithm	Implementation	MBF [kW/m^2]	SR [–]
GA	I	16.938	0/3
	II	17.005	0/3
	III	17.535	0/3
	IV	17.794	0/3
	V	17.243	0/3
PSO	I	17.901	1/3
	II	17.978	1/3
	III	18.802	2/3
	IV	16.336	0/3
	V	17.482	0/3
	VI	16.578	0/3
	VII	18.642	2/3
	VIII	19.450	3/3
	IX	17.088	1/3

Table A.20
Mean Best Fitness (MBF) and Success Rate (SR) for all algorithms applied to objective function $f_5 = \bar{P}/S$ for a device oscillating in surge only.

Algorithm	Implementation	MBF [kW/m^2]	SR [–]
GA	I	515.265	3/3
	II	515.346	3/3
	III	515.862	3/3
	IV	517.412	3/3
	V	516.145	3/3
PSO	I	512.556	3/3
	II	512.952	3/3
	III	516.646	3/3
	IV	509.957	3/3
	V	516.223	3/3
	VI	514.651	3/3
	VII	514.637	3/3
	VIII	507.149	3/3
	IX	510.017	3/3

Table A.21
Mean Best Fitness (MBF) and Success Rate (SR) for all algorithms applied to objective function $f_5 = -\bar{P}/S$ for a device oscillating in surge, heave and pitch.

Algorithm	Implementation	MBF [kW/m^2]	SR [–]
GA	I	2751.441	3/3
	II	2752.951	2/3
	III	2779.303	2/3
	IV	2739.368	2/3
	V	2762.598	2/3
PSO	I	2852.934	3/3
	II	2851.767	3/3
	III	2872.462	3/3
	IV	2625.956	0/3
	V	2818.093	3/3
	VI	2729.297	2/3
	VII	2786.743	2/3
	VIII	2805.595	2/3
	IX	2799.169	3/3

Table A.22
Mean Best Fitness (MBF) and Success Rate (SR) for all algorithms applied to objective function $f_6 = -\bar{P}/S^{\frac{1}{2}}$ for a device oscillating in surge only.

Algorithm	Implementation	MBF [kW/m]	SR [–]
GA	I	11.781	1/3
	II	11.721	2/3
	III	12.061	2/3
	IV	12.023	2/3
	V	11.798	1/3
PSO	I	11.997	2/3
	II	12.187	3/3
	III	12.074	3/3
	IV	11.843	2/3
	V	12.074	2/3
	VI	11.777	3/3
	VII	12.130	3/3
	VIII	12.203	3/3
	IX	11.781	3/3

Table A.23
Mean Best Fitness (MBF) and Success Rate (SR) for all algorithms applied to objective function $f_6 = -\bar{P}/S^{\frac{1}{2}}$ for a device oscillating in surge only.

Algorithm	Implementation	MBF [kW/m]	SR [–]
GA	I	39.332	2/3
	II	39.334	0
	III	38.288	0
	IV	38.208	0
	V	38.637	1/3
PSO	I	39.829	2/3
	II	38.660	1/3
	III	39.526	1/3
	IV	37.952	0
	V	38.610	0
	VI	39.242	1/3
	VII	40.239	2/3
	VIII	40.317	2/3
	IX	38.500	1/3

References

[1] Nguyen AT, Reiter S, Rigo P. A review on simulation-based optimization methods applied to building performance analysis. Appl Energy 2014;113:1043–58. http://dx.doi.org/10.1016/j.apenergy.2013.08.061.

[2] Yang H, Wei Z, Chengzhi L. Optimal design and techno-economic analysis of a hybrid solar-wind power generation system. Appl Energy 2009;86(2):163–9. http://dx.doi.org/10.1016/j.apenergy.2008.03.008.

[3] Ekren O, Ekren BY. Size optimization of a PV/wind hybrid energy conversion system with battery storage using simulated annealing. Appl Energy 2010;87(2):592–8. http://dx.doi.org/10.1016/j.apenergy.2009.05.022.

[4] Wang JJ, Jing YY, Zhang CF. Optimization of capacity and operation for CCHP system by genetic algorithm. Appl Energy 2010;87(4):1325–35. http://dx.doi.org/10.1016/j.apenergy.2009.08.005.

[5] Strategic Initiative for Ocean Energy (SI OCEAN). Ocean energy: Cost of energy and cost reduction opportunities. SI OCEAN; 2013, May.

[6] Bull D, Ochs ME, Laird DL, Boren B, Jepsen RA. Technological cost-reduction pathways for oscillating water column wave energy converters in the marine hydrokinetic environment. 2013, p. 1–50. http://dx.doi.org/10.2172/1092993, September.

[7] Gilloteaux J-C, Ringwood J. Control-informed geometric optimisation of wave energy converters. IFAC Proc Vol 2010;(20):366–71. http://dx.doi.org/10.3182/20100915-3-DE-3008.00072.

[8] Kurniawan A, Moan T. Multi-objective optimization of a wave energy absorber geometry. In: Proc. of the 27th international workshop on water waves and floating bodies. no. 2. 2012. p. 3–6.

[9] Kurniawan A, Moan T. Optimal geometries for wave absorbers oscillating about a fixed axis. IEEE J Ocean Eng 2013;38(1):117–30. http://dx.doi.org/10.1109/JOE.2012.2208666.

[10] Costello R, Teillant B, Weber J, Ringwood JV. Techno-economic optimisation for wave energy converters. In: Proc. of the 4th international conference on ocean energy. 2012.

[11] Blanco M, Lafoz M, Navarro G. Wave energy converter dimensioning constrained by location, power take-off and control strategy. In: Proc. of 2012 IEEE international symposium on industrial electronics. IEEE; 2012, p. 1462–7. http://dx.doi.org/10.1109/ISIE.2012.6237307.

[12] Weber J, Thomas GP. Turbine type & design selection in the context of multi-parametric overall system optimisation of Oscillating Water Column wave energy converters Introduction & Motivation. In: Proc. of the international conference on ocean energy. Bremerhaven, Germany. 2006.

[13] Pillai AC, Thies PR, Johanning L. Mooring system design optimization using a surrogate assisted multi-objective genetic algorithm. Eng Optim 2018;1–23. http://dx.doi.org/10.1080/0305215X.2018.1519559.

[14] McCabe AP, Aggidis GA, Widden MB. Optimizing the shape of a surge-and-pitch wave energy collector using a genetic algorithm. Renew Energy 2010;35(12):2767–75. http://dx.doi.org/10.1016/j.renene.2010.04.029.

[15] McCabe AP. Constrained optimization of the shape of a wave energy collector by genetic algorithm. Renew Energy 2013;51:274–84. http://dx.doi.org/10.1016/j.renene.2012.09.054.

[16] Weber J, Thomas GP. An efficient flexible engineering tool for multi-parametric hydrodynamic analysis in the design & optimisation of WECs. In: Proc. of the 6th European wave and tidal energy conference. Glasgow, Scotland. 2005. p. 543–48.

[17] Garcia-Teruel A, DuPont B, Forehand DIM. Hull geometry optimisation of wave energy converters: on the choice of the optimisation algorithm and the geometry definition. In: figshare. 2020, http://dx.doi.org/10.6084/m9.figshare.13070234.v1.

[18] Papalambros PY, Wilde DJ. Principles of optimal design: Modeling and computation. Cambridge University Press; 2000, p. 416.
[19] Garcia-Teruel A, Forehand DIM. Optimal wave energy converter geometry for different modes of motion. In: Advances in renewable energies offshore: Proceedings of the 3rd international conference on renewable energies offshore. Lisbon. 2018. p. 299–05.
[20] Tucker M, Pitt E. Waves in ocean engineering. Elsevier Science; 2001.
[21] Cahill B, Lewis T. Wave period ratios and the calculation of wave power. In: Proc. of the 2nd marine energy technology symposium. Seattle. 2014.
[22] Falnes J. Ocean waves and oscillating systems. New York: Cambridge University Press; 2002.
[23] Babarit A, Clément AH. Shape optimisation of the SEAREV wave energy converter. In: Proc. of the 9th World renewable energy congress. 2006.
[24] Gomes R, Henriques J, Gato L, Falcão A. Hydrodynamic optimization of an axisymmetric floating oscillating water column for wave energy conversion. Renew Energy 2012;44:328–39. http://dx.doi.org/10.1016/J.RENENE.2012.01.105.
[25] Blum C, Roli A. Metaheuristics in combinatorial optimization. ACM Comput Surv 2003;35(3):268–308. http://dx.doi.org/10.1145/937503.937505.
[26] Ribeiro E Silva S, Gomes RP, Falcaõ AF. Hydrodynamic optimization of the UGEN: Wave energy converter with U-shaped interior oscillating water column. Int J Mar Energy 2016;15:112–26. http://dx.doi.org/10.1016/j.ijome.2016.04.013.
[27] Baker J. Reducing bias and inefficiency in the selection algorithm. In: Proc. of the 2nd international conference on genetic algortihms and their applications. Hillsdale, NJ. 1987. p. 14–21.
[28] Mühlenbein H, Schlierkamp-Voosen D. Predictive models for the breeder genetic algorithm. Evol Comput 1993;1(1):25–49. http://dx.doi.org/10.1162/evco.1993.1.1.25.
[29] MIT. WAMIT user manual. URL http://www.wamit.com/manualupdate/V70_manual.pdf.
[30] Maniar HD. A three dimensional higher order panel method based on B-splines (Ph.D. thesis), Massachusetts Institute of Technology; 1995, URL https://dspace.mit.edu/handle/1721.1/11127.
[31] Rogers DF, Adams JA. Mathematical elements for computer graphics. McGraw-Hill Book Company; 1976.
[32] Babarit A, Hals J, Muliawan M, Kurniawan A, Moan T, Krokstad J. Numerical benchmarking study of a selection of wave energy converters. Renew Energy 2012;41:44–63. http://dx.doi.org/10.1016/j.renene.2011.10.002.
[33] de Andres A, Maillet J, Todalshaug JH, Möller P, Jeffrey H. On the optimum sizing of a real WEC from a techno- economic perspective. In: International conference on ocean, offshore and arctic engineering. 2016.
[34] Kalofotias F. Study for the hull shape of a wave energy converter-point absorber design optimization & modeling improvement (Msc thesis), (June):University of Twente; 2016, p. 37.
[35] Guanche R, Gómez V, Vidal C, Eguinoa I. Numerical analysis and performance optimization of a submerged wave energy point absorber. Ocean Eng 2013;59:214–30. http://dx.doi.org/10.1016/J.OCEANENG.2012.10.016.
[36] Madhi F, Sinclair ME, Yeung RW. The "Berkeley Wedge": an asymmetrical energy-capturing floating breakwater of high performance. Mar Syst Ocean Technol 2014;9(1):5–16.
[37] Babarit A. A database of capture width ratio of wave energy converters. Renew Energy 2015;80:610–28. http://dx.doi.org/10.1016/j.renene.2015.02.049.
[38] Chipperfield A, Fleming P, Pohlheim H, Fonseca C. Genetic algorithm toolbox - User's guide. University of Sheffield; 1995.
[39] Perez R, Behdinan K. Particle swarm approach for structural design optimization. Comput Struct 2007;85(19–20):1579–88. http://dx.doi.org/10.1016/J.COMPSTRUC.2006.10.013.
[40] del Valle Y, Venayagamoorthy G, Mohagheghi S, Hernandez J-C, Harley R. Particle swarm optimization: Basic concepts, variants and applications in power systems. IEEE Trans Evol Comput 2008;12(2):171–95. http://dx.doi.org/10.1109/TEVC.2007.896686.
[41] Constrained particle swarm optimization, version 1.31.2. In: Mathworks file exchange. 2016, URL https://uk.mathworks.com/matlabcentral/fileexchange/25986-constrained-particle-swarm-optimization.
[42] Eiben AE, Smith JE. Introduction to evolutionary computing techniques. 2nd ed.. Berlin Heidelberg: Springer; 2012, http://dx.doi.org/10.1109/etd.1995.403482.